ADVANCED ENERGY MATERIALS

Supporting Information

for *Adv. Energy Mater.,* DOI: 10.1002/aenm.202102122

Multiphase, Multiscale Chemomechanics at Extreme Low Temperatures: Battery Electrodes for Operation in a Wide Temperature Range

Jizhou Li, Shaofeng Li, Yuxin Zhang, Yang Yang, Silvia Russi, Guannan Qian, Linqin Mu, Sang-Jun Lee, Zhijie Yang, Jun-Sik Lee, Piero Pianetta, Jieshan Qiu, Daniel Ratner, Peter Cloetens, Kejie Zhao,* Feng Lin,* and Yijin Liu**

Supporting Information

Multiphase, multiscale chemomechanics at extreme low temperatures: battery electrodes for operation in a wide temperature range

Jizhou Li, Shaofeng Li, Yuxin Zhang, Yang Yang, Silvia Russi, Guannan Qian, Linqin Mu, Sang-Jun Lee, Zhijie Yang, Jun-Sik Lee, Piero Pianetta, Jieshan Qiu, Daniel Ratner, Peter Cloetens, Kejie Zhao*, Feng Lin*, Yijin Liu**

Table S1. EXAFS fitting results for the structural parameters around Ni under different stages.

Sample	Path	N	R(Å)	σ^2 (10^{-3}Å)	ΔE_0 (eV)	R-factor
298 K	Ni-O	4.0±0.1	1.89±0.01	5.2±0.4	1.0±0.4	0.006
	Ni-M	5.1±0.1	2.85±0.01	5.3±0.4	0.2±0.4	
100 K	Ni-O	3.9±0.1	1.94±0.01	4.5±0.6	1.4±0.5	0.009
	Ni-M	5.5±0.1	2.81±0.01	4.5±0.5	-0.5±0.4	
Recovery	Ni-O	4.0±0.1	1.90±0.01	4.7±1.3	0.7±0.4	0.006
	Ni-M	5.1±0.1	2.84±0.01	5.3±0.5	0.3±0.4	

N is the coordination number; *R* is interatomic distance (the bond length between Co central atoms and surrounding coordination atoms; σ^2 is Debye-Waller factor (represents the thermal and static disorder in absorber-scatterer distances); ΔE_0 is edge-energy shift (the difference between the zero kinetic energy value of the sample and that of the theoretical model). *R* factor is used to assess the goodness of the fitting.

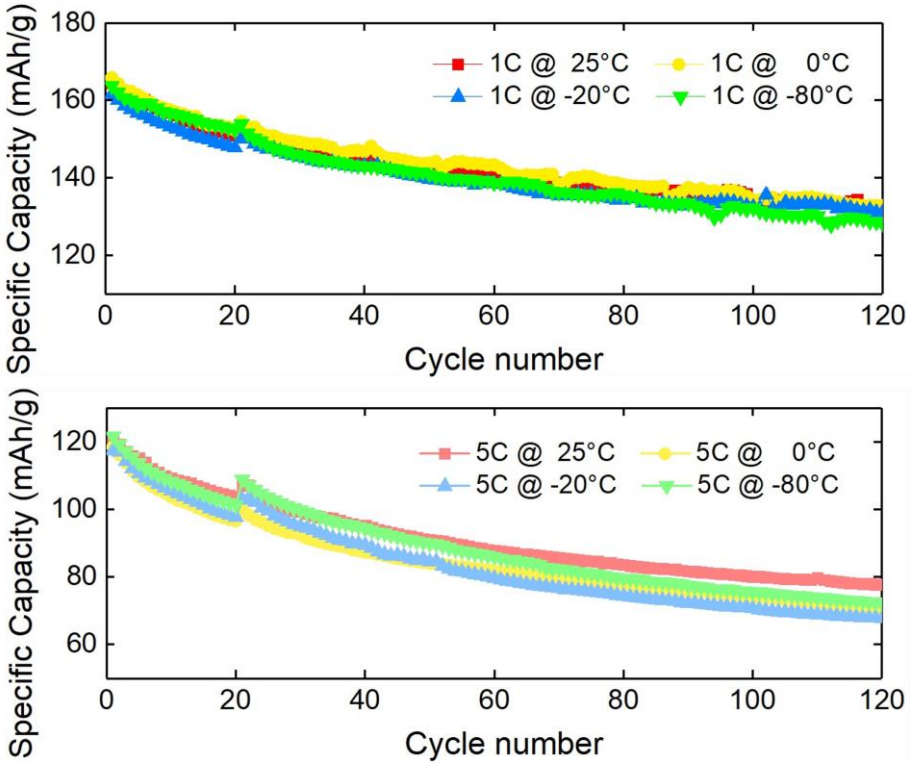

Figure S1. The electrochemical performance of Li/NMC half-cells upon storage at different temperatures (25 °C, 0 °C, -20 °C, and -80 °C).

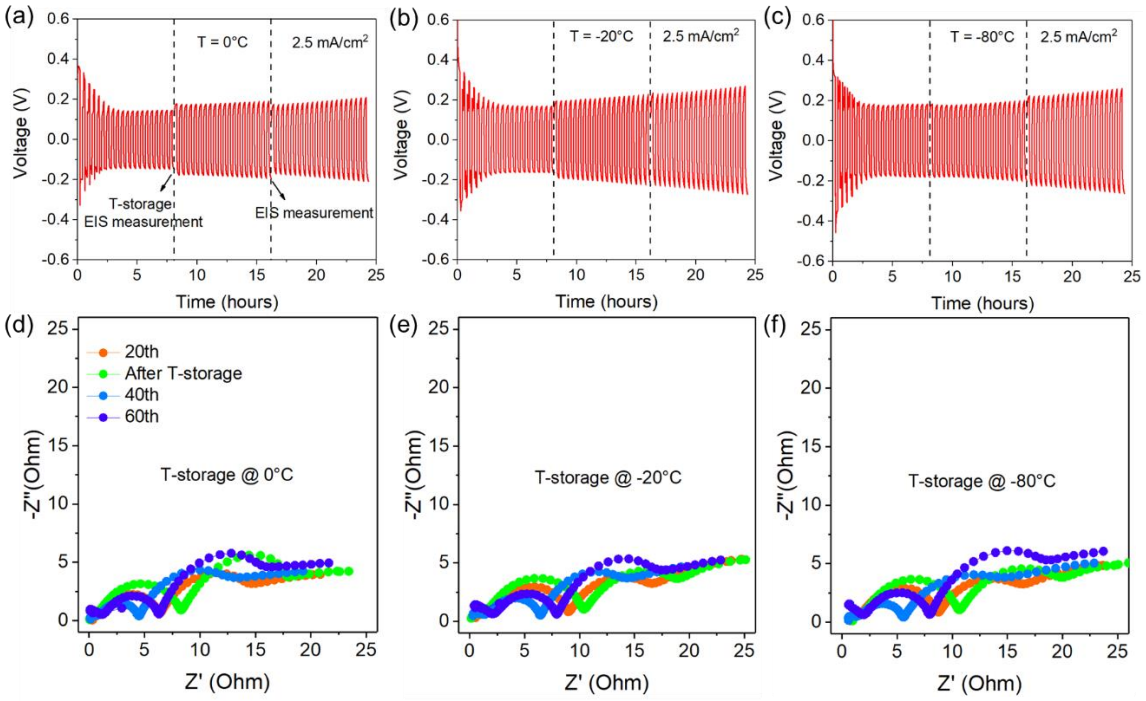

Figure S2. The electrochemical performance of Li symmetrical cells upon storage at different temperatures (0 °C, -20 °C, and -80 °C). Voltage-time profiles of the symmetric cell stored at (a) 0 °C, (b) -20 °C and (c) -80 °C at 2.5 mA/cm^2. The cells are firstly activated for one cycle using a small current density (0.05 mA/cm^2) and followed by 20 cycles of fast charging-discharging at 25 °C (~8 hours). Then these cells are stored at different temperatures for 2 days and rested at room temperature for 2 days for further electrochemical measurements. The electrochemical impedance spectra of the Li symmetric cells stored at (d) 0°C, (e) -20°C and (f) -80 °C. 20th indicates the first 20 cycles at room temperature for different cells, and 40th indicates 20 cycles at room temperature plus 20 cycles after T-storage. The similar results among different cells suggest negligible impact coming from Li-metal anode.

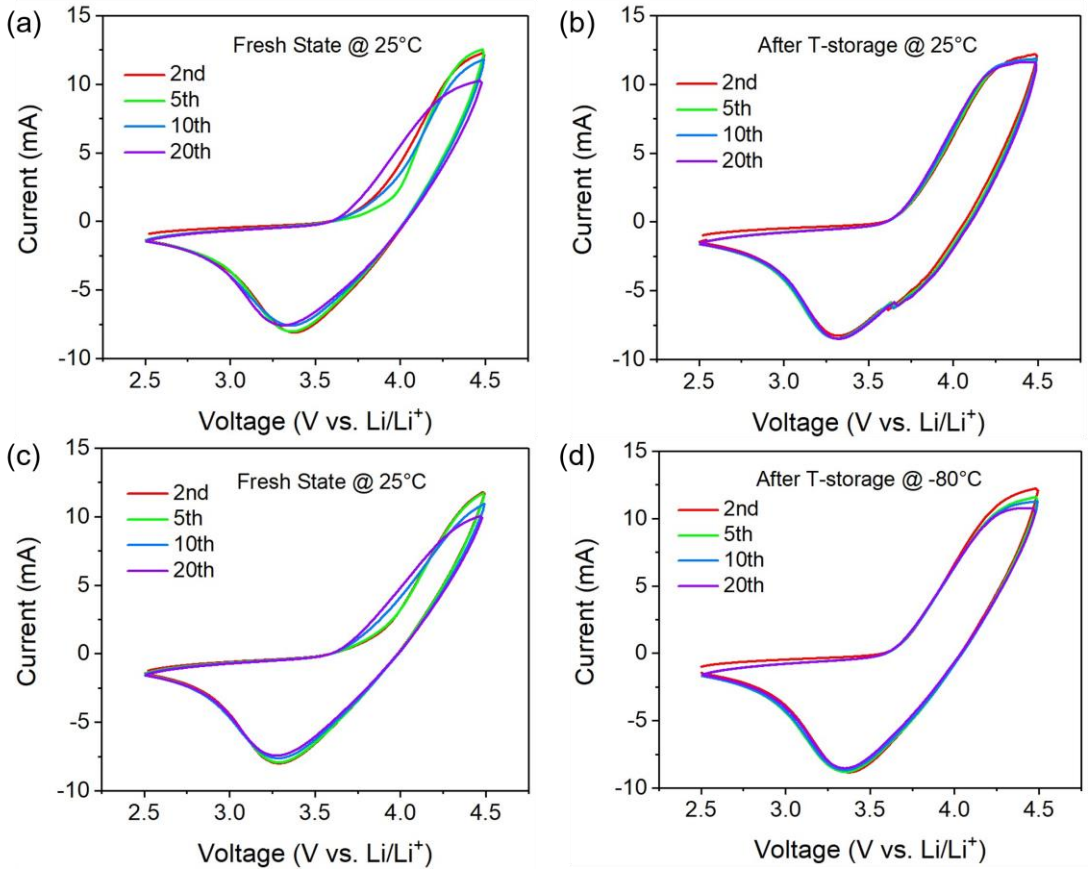

Figure S3. CV profiles of Li/NMC half-cell upon storage at 25 °C and -80 °C. Two cells are firstly cycled at 25 °C and the results are shown in (a) and (c). Following CV measurements are performed on these cells after being stored at (b) 25 °C and (d) -80 °C. Current drop at high-voltage can still be observed after low-temperature storage. The voltage range is 2.5 – 4.5 V and the scan rate is 5 mV/s upon the CV measurements.

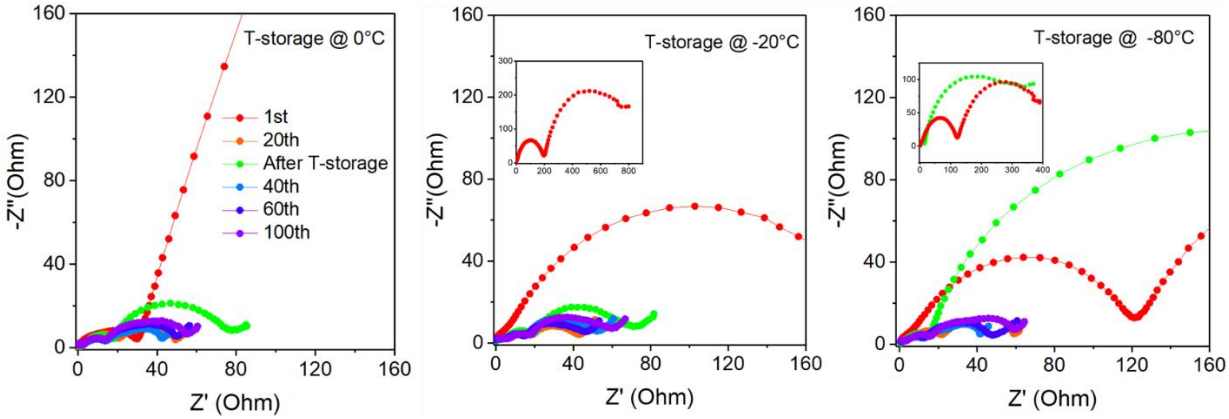

Figure S4. The electrochemical impedance spectra of Li/NMC half-cell upon storage at low temperatures (0 °C, -20 °C and -80 °C). First cycle is a formation cycle using a current density of 20 mA/g (1st). Then the cells are electrochemically cycled at 5C (1A/g) for 20 times (20th), after which they are stored at different temperatures for 2 days and rested at 25°C for 2 days for EIS measurements (After T-storage). 40th, 60th and 100th indicates 20 cycles at room temperature plus 20, 40 and 60 cycles after T-storage. The charge transfer resistance is enlarged after low-temperature storage, especially at -80 °C.

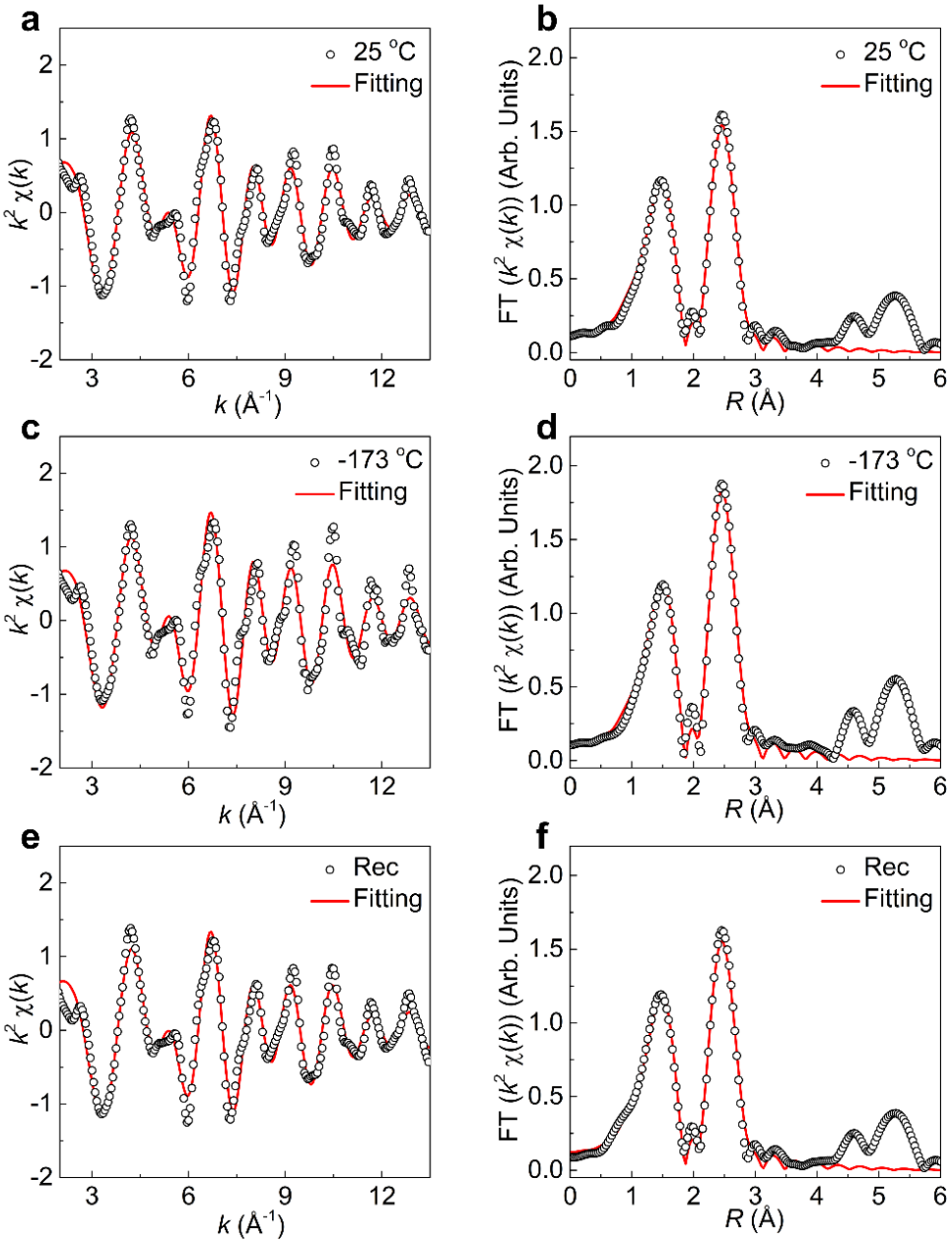

Figure S5. EXAFS $k^2\chi(k)$ oscillation curves and R space fitting results of Ni K-edge for the electrodes under different conditions: a, b) RT, c, d) Low-T and e, f) recovery.

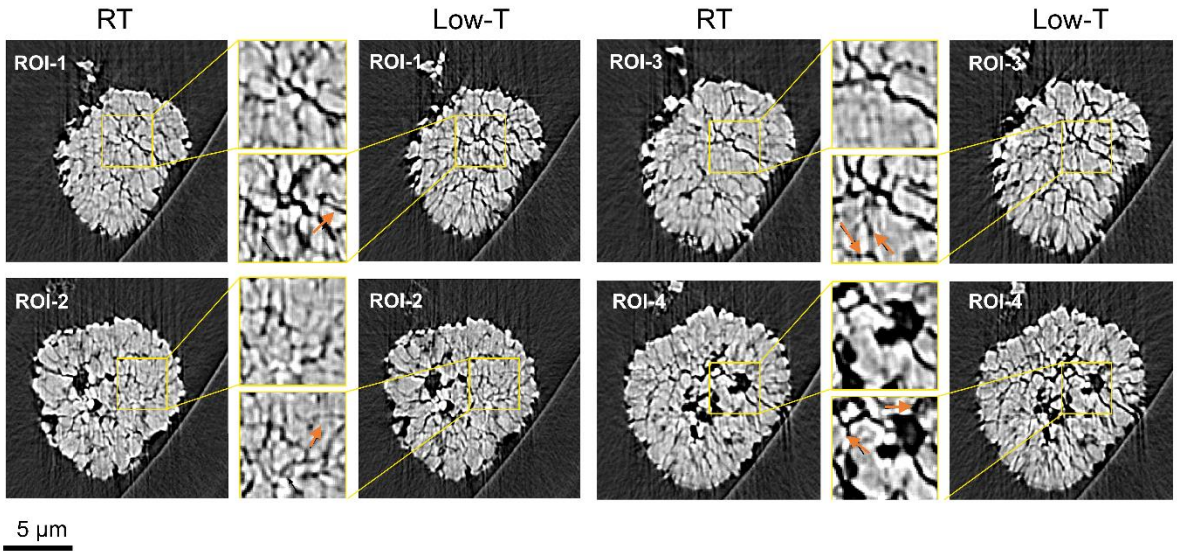

Figure S6. Example ROIs of the mesoscale particle cracking at RT and low-T conditions. They are visualized by the transmission x-ray microscopy.

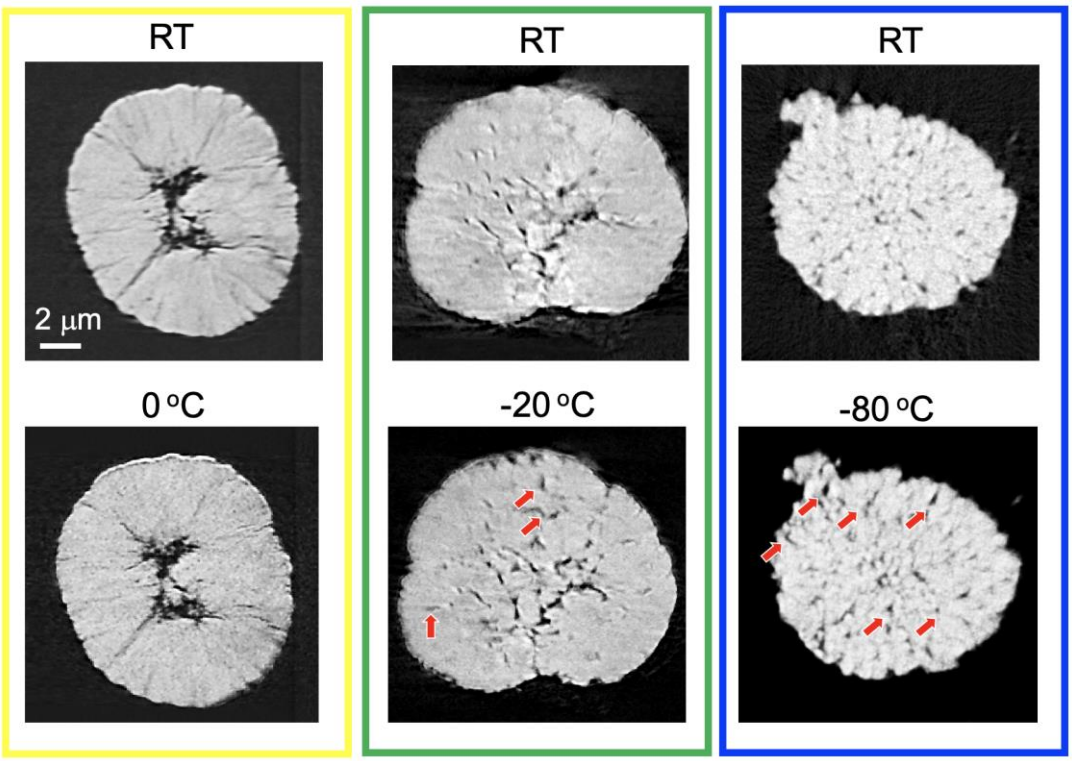

Figure S7. In-situ TXM imaging of single NMC particles upon exposure to different temperatures (0 °C, -20 °C, and -80 °C) for one hour. Zero-degree Celsius exposure does not induce further cracks. The exposure to -20 °C and -80 °C both cause the particles to further damage.

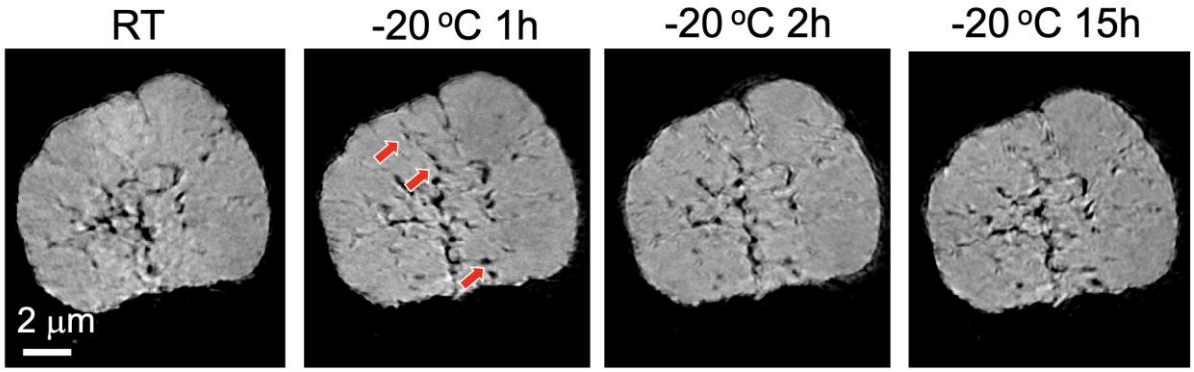

Figure S8. In-situ TXM imaging of a single NMC particle under -20 °C for different amounts of time (1 hour, 2 hours, and 15 hours). The low-T induced further particle damage already appear when the particle is exposed to -20 °C for 1 hour. Further temperature hold does not induce more damages.

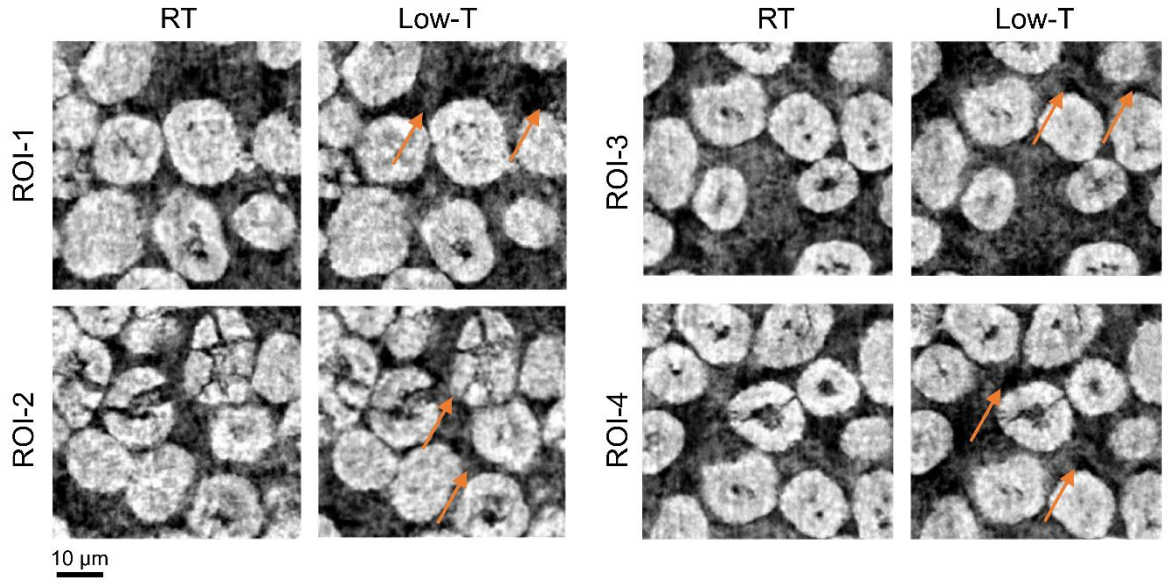

Figure S9. Example ROIs of the cathode deformation at RT and low-T conditions. They are visualized by x-ray phase contrast nano-tomography.

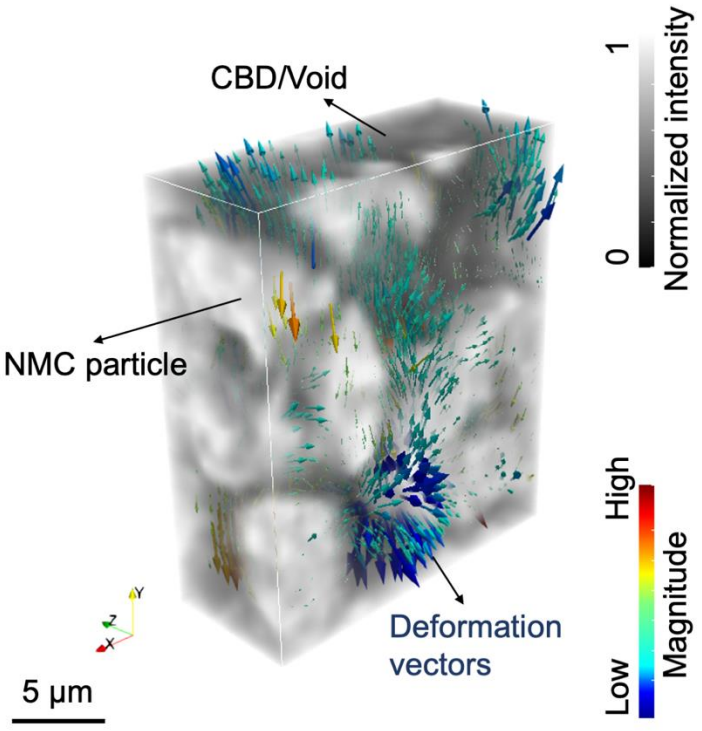

Figure S10. 3D visualization of the deformation of the cathode part after exposure to the low-temperature environment. The raw tomography data (grayscale, normalized intensity) is overlayed by the deformation vectors. The deformation magnitude is proportional to the size of quivers (with 2x magnification for better visualization), and color coded. Higher value of deformation magnitude is represented by 'red' and lower value by 'blue' color respectively. The quivers also show the direction of the displacement.

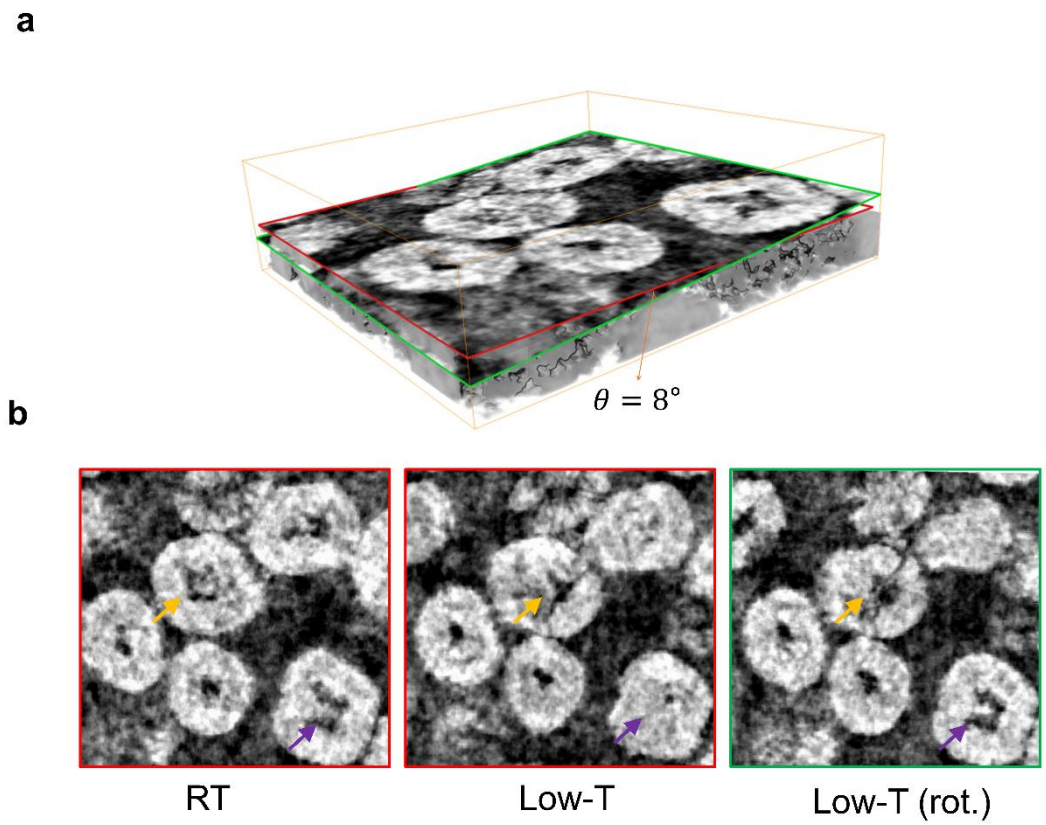

Figure S11. Demonstration of particle rotation after exposure to low-temperature condition. The whole volumes in RT and low-T are globally optimally registered, while individual particles are observed to be inconsistent on their inner structures. This noticeable difference can be verified by rotating the plane (e.g. 8°) from the RT condition ('red' box) to the low-T condition ('green' box). Some particles (e.g. 'purple' arrow indicated) are structurally similar in both conditions, while others (e.g. 'yellow' arrow indicated) are still not. This confirms the complicated structural deformation in the electrode after the exposure to low-temperature.

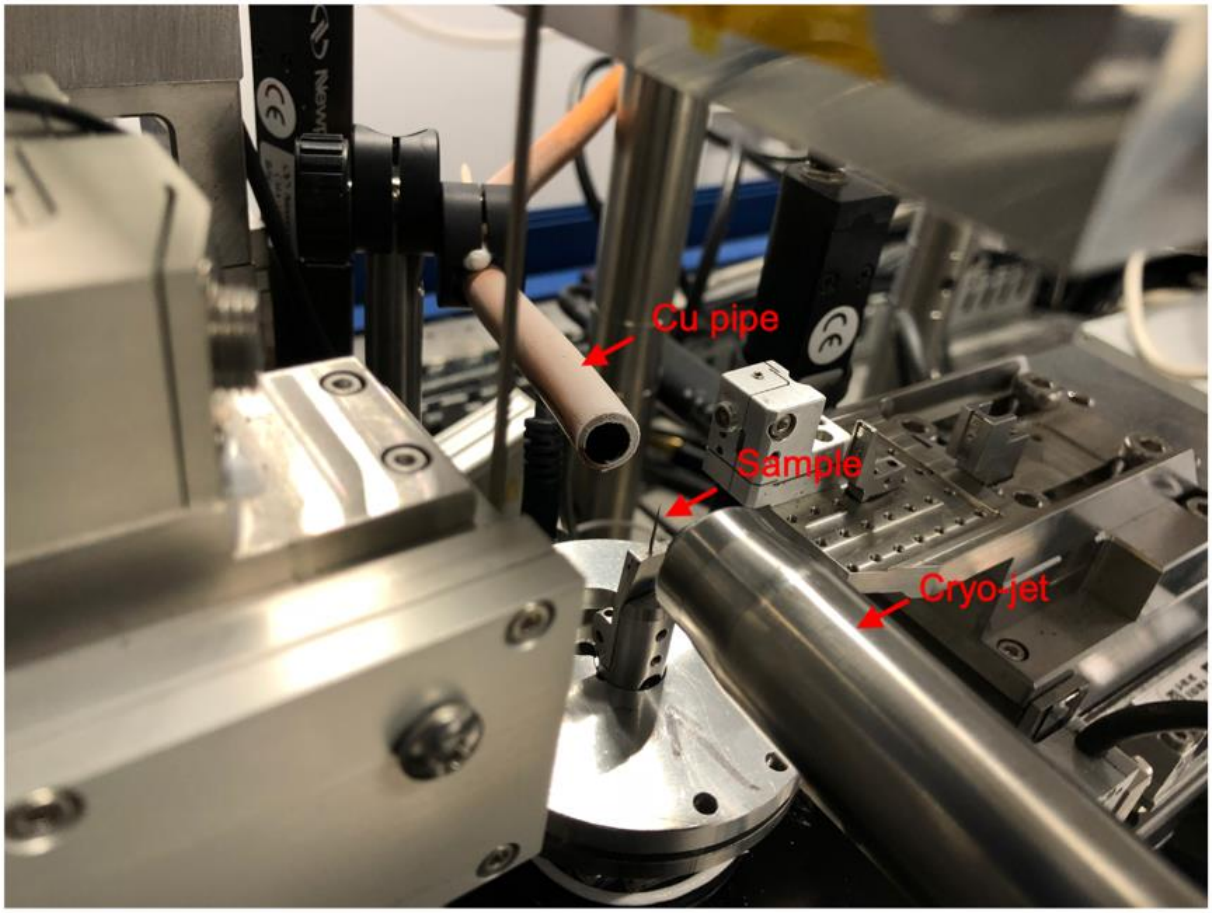

Figure S12. Experimental setup for the TXM imaging. The cryo-jet is used to deliver cold air on one side of the sample. A Cu pipe (connected to a vacuum cleaner) to suck the cold air away on the other side of the sample. The cryo-jet delivers cold air with dry N2 shielding to avoid sample icing.

Supplementary Note

Clarification on the selection of temperature points in the experiments

First of all, while we appreciate that a careful temperature calibration is important and has been done properly in our experiments, it is our opinion that the absolute temperature value is not the scientific focus of our research. Instead, we look into the low-temperature-induced chemomechanical damages to the battery electrode at multiple length scales and the overall trend offers the most valuable information for our understanding of the degradation mechanism under low temperature.

Second, the multi-modal in-situ synchrotron characterizations under low-temperature conditions conducted in this work come with experimental challenges and constrains. For example, the low-temperature XRD experiment is the least time-consuming experiment. We conducted the low-T XRD at a beamline that was designed for protein crystallography under cryogenic conditions and, therefore, the temperature can be precisely and conveniently controlled. Our low-T XRD was carried out with a temperature step of ~50 degrees: RT (~25 °C), -23 °C, -73 °C, -123 °C -153 °C, -173 °C. Our data suggest that the low-T-induced lattice contraction saturates at around -73 °C. With this information as input, we then carried out those more time-consuming characterizations at fewer temperature points, e.g. XANES and EXAFS at RT and -173 °C, TXM at RT, -20 °C, -40 °C and -80 °C, nano-holo-tomography at RT and -133 °C.

We essentially compared the spectroscopy (XANES and EXAFS) and imaging (TXM and phase-contrast nano-tomography) data above and below this saturation point, which helps us to understand the low-T-induced electrode degradation.